Nuclear Engineering and Technology 57 (2025) 103329

Contents lists available at ScienceDirect

Nuclear Engineering and Technology

journal homepage: www.elsevier.com/locate/net

Original Article

Pulse pile-up recognition using multi-module DenseNet in neutron-gamma discrimination

Ye Pan [a], Pin Gong [a,b,*], Zhimeng Hu [a,b], Zeyu Wang [a], Dajian Liang [a], Cheng Zhou [c], Xiaoxiang Zhu [c], Xiaobin Tang [a,b]

[a] Department of Nuclear Science and Technology, Nanjing University of Aeronautics and Astronautics, Nanjing, 210016, China
[b] Key Laboratory of Nuclear Technology Application and Radiation Protection in Aerospace, Ministry of Industry and Information Technology, Nanjing University of Aeronautics and Astronautics, Nanjing, 210016, China
[c] Jiangsu Nuclear and Radiation Safety Supervision and Management Center, Nanjing, 210019, China

ARTICLE INFO

Keywords:
Neutron detection
Pulse piled-up recognition
EJ301
DenseNet
MMDenseNet

ABSTRACT

Neutron-gamma discrimination is crucial for various applications in nuclear science and technology. Currently, the majority of research is focused on pulse shape discrimination, and conventional methods achieve a certain level of accuracy in conventional neutron-gamma discrimination scenarios. However, under high-count-rate conditions, neutron-gamma signals tend to pile-up, resulting in pulse shape changes, that significantly affect the accuracy of conventional methods. In recent years, neural network technology has been shown to be effective for signal waveform recognition.

In this study, two Multi-Module DenseNet network structures were designed: Multi-module DenseNet (MMDenseNet) and Multi-module DenseNet with base layer Reuse (MMDenseNet-R). The accuracy and F1-score of MMDenseNet/MMDenseNet-R for recognizing piled-up pulses at different pile-up degrees and noise levels was evaluated using DenseNet and ResNet as comparison networks. Among the various pile-up cases examined in this study, MMDenseNet/MMDenseNet-R consistently outperformed ResNet and DenseNet, showing clear superiority over conventional pulse shape discrimination methods.

MMDenseNet/MMDenseNet-R achieved high-precision pulse piled-up recognition under various pile-up conditions through their modular design, thereby improving the usage of piled-up pulses during detection. These network architectures are expected to acquire more valid signals in complex neutron fields, further optimizing the accuracy of particle detection.

1. Introduction

Neutron-gamma discrimination is an important aspect of neutron detection, which plays a crucial role in nuclear physics research, nuclear medicine, radiation monitoring, nuclear security, non-proliferation and nuclear facility security measures. Currently, most studies on neutron-gamma discrimination focus on pulse shape discrimination (PSD) methods [1]. Common techniques include charge comparison [2], rise -time [3], and the zero-crossing methods [4]. These methods discriminate between neutron and gamma signals by using their unique waveform characteristics. In addition, neural network technologies have shown excellent capabilities in the field of neutron-gamma discrimination, with convolution neural network(CNN) [5] and Residual Network (ResNet) [6]demonstrating particularly good discrimination abilities.

However, under high-count-rate conditions [7], multiple signals tend to pile up, resulting in piled-up pulse signals. Typically, at count rates of approximately 100–200 KCps (kilo counts per second) or higher, the count rate reaches the limit that the electronics and scintillator can handle within the time resolution window, and the probability of pulse pile-up increases significantly. Conventional PSD methods cannot accurately recognize piled-up pulse signals, and current equipment can only discard them directly. In 2022, Song [8] conducted research on pulse pile-up recognition using ResNet and achieved more than 98 % accuracy and F1 scores under certain pile-up conditions. By recognizing these piled-up pulses, more information can be extracted from otherwise invalid signals, which can then be converted into invalid signals.

To comprehensively simulate real neutron detection environments, the degree of pulse pile-up and noise levels were categoried into three

* Corresponding author. Department of Nuclear Science and Technology, Nanjing University of Aeronautics and Astronautics, Nanjing, 210016, China.
E-mail address: gongpin@nuaa.edu.cn (P. Gong).

https://doi.org/10.1016/j.net.2024.11.031
Received 28 August 2024; Received in revised form 7 November 2024; Accepted 18 November 2024
Available online 19 November 2024

different grades, resulting in nine pile-up conditions for the experiments. In this study, DenseNet [9] was used for pulse piled-up recognition and a modular design was proposed to construct a new neural network model, multi-module DenseNet (MMDenseNet). This structure can automatically select network branches for piled-up pulse recognition based on different pile-up conditions, thereby improving the recognition accuracy compared to DenseNet.

In this study, an EJ301 liquid scintillation detector was used to detect signals from an Am-Be source. After training and testing the neural networks, Accuracy and F1 score were selected as performance evaluation metrics for further analysis.

2. Materials and method

The process of the MMDenseNet pile-up pulse recognition method proposed in this study is shown in Fig. 1 and mainly consists of three parts: experimental setup and creation of the neutron/gamma signal dataset, creation of the pile-up pulse dataset, and construction, training, and testing of the neural networks. First, a dataset of neutron/gamma signals was created using an Am-Be source and an EJ301 detector in combination with a time-of-flight (TOF) [10] and charge comparison method (CCM) [3]. Subsequently, these signals underwent signal shifting and addition to generate a pile-up pulse dataset consisting of four types: neutron-neutron, neutron-gamma, gamma-neutron, and gamma-gamma. The pile-up pulse dataset is further expanded by controlling the time intervals and adding varying noise levels to create a complete pile-up pulse dataset. Finally, the DenseNet, MMDenseNet, and MMDenseNet-R networks were separately trained and tested. The performance of the model was evaluated under nine pile-up conditions based on accuracy and F1 score and compared with ResNet. The entire process was executed on a Windows operating system using Python as the programming language and PyTorch as the deep learning framework. Detailed explanations of these three aspects can be found below:

2.1. Part I: Experimental setup and creation of the neutron/gamma signal dataset

In this study, EJ301 liquid scintillator detectors (M515-20x20-6, 20in×20in, 106 mL) with a time-of-flight method were used for signal acquisition. The source used in the experiment was an Am-Be source (1.08×10^6 n/s.; 0–11.0 MeV, with an average energy of approximately 4.5 MeV) from the State Key Laboratory of Nuclear Physics and Technology, Peking University [11].

In the experiment (Fig. 2a), two EJ-301 liquid scintillator(Fig. 2b) detectors were used for coincidence counting [11,12]. Detector A, serving as the start detector, was placed close to the AmBe neutron source, while Detector B, serving as the stop detector, was positioned 1 m away from the source. They provided the start and stop times for the TOF measurement. Table 1 shows the start and stop times and times of flight for the first ten signals measured using the TOF method. Since Detectors A and B are positioned on opposite sides of the AmBe source, negative time of flight values may occur.

A high-voltage power supply provided −1520V to the ET9814B photomultiplier tube (PMT) to convert the light signals generated by the neutrons hitting the scintillator into negative pulses. These negative pulses were then digitized using a CAEN DT5720 digitizer and sent to a PC for processing and analysis. The DT5720 digitizer has a 2V peak-to-peak dynamic range and a 12-bit resolution, providing 4096 levels of quantization for digitizing signals, with a threshold of 0.5 mV. The digitizer offers a 250 MS/s sampling rate, meaning it can capture 250 million samples per second.

During the signal acquisition process, there is a significant difference in the falling edges of neutron and gamma signals collected using the

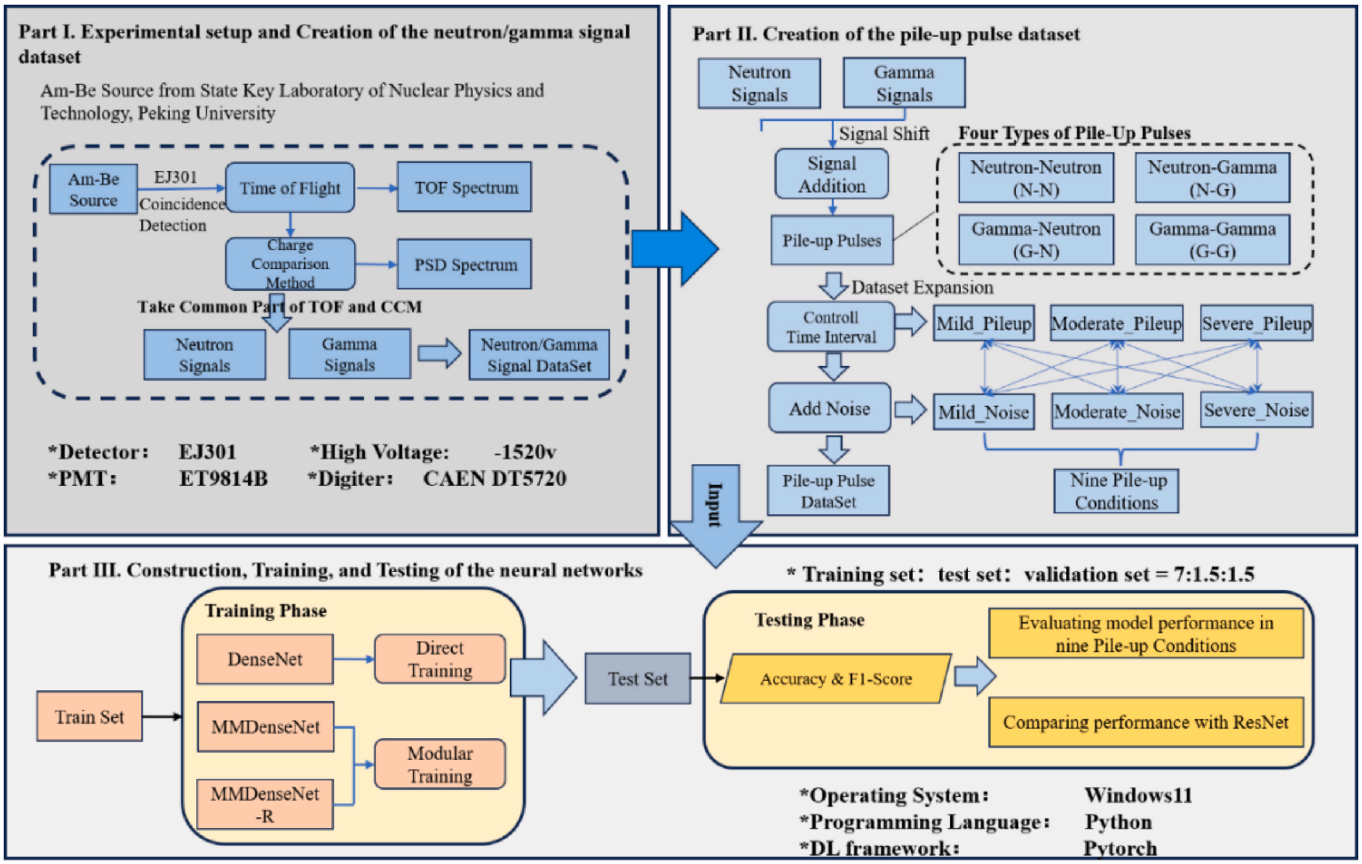

Fig. 1. Pulse piled-up recognition process.

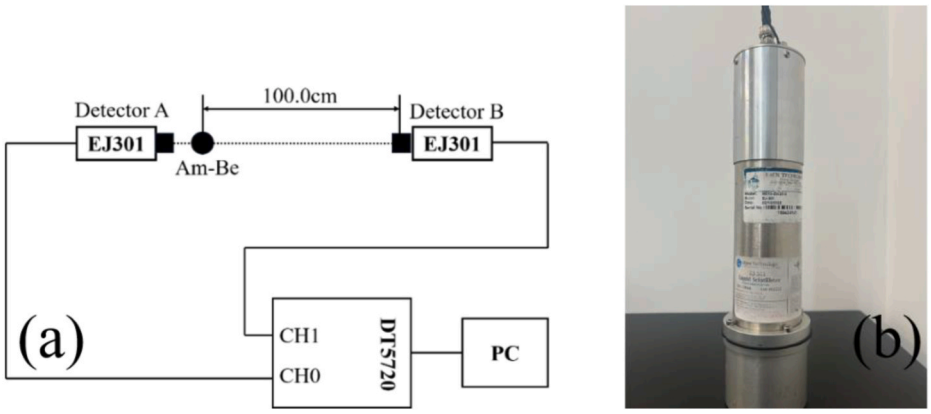

Fig. 2. Time-of-flight Experimental Setup (a) and EJ301 liquid scintillator (b).

Table 1
Timing for the first ten signals in TOF.

Number	Start time(ps)	Stop time(ps)	Time of flight(ps)
1	160211554499	160211480249	−74250
2	946772449000	946772290000	−159000
3	1196342822249	1196342804249	−18000
4	1509836920749	1509837132749	212000
5	1769628514749	1769628588249	73500
6	2182184306374	2182184540749	234375
7	2741037245249	2741037258000	12751
8	3243090130749	3243090119000	−11749
9	3344661456749	3344661416000	−40749
10	3431388105000	3431388036000	−69000

EJ301 liquid scintillator detector, as shown in Fig. 3. The complete information of the rising and falling edges of both signals can be fully captured within a 100 ns time window. In this study, a unified time window of 120 ns was selected for analysis.

Fig. 4a shows the time-of-flight spectra. The counting and statistical analysis of the flight times of the collected signals yielded the time-of-flight spectra. The main peak at a flight time close to zero corresponds to gamma events, whereas the second peak at longer flight times reflects neutron events. In this experiment, the time range of [−25∼-3] ns was defined as gamma ray signals and [10–50] ns as neutron signals, the background in Fig. 4 is the random coincidences. To further avoid random coincidences in the coincidence method, a charge comparison method was used to further discriminate between the neutron and gamma signals collected by the time-of-flight method.

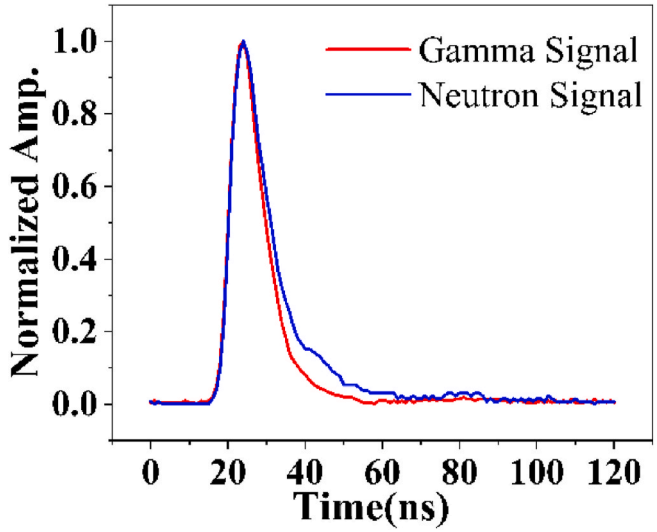

Fig. 3. Neutron/Gamma timing signal diagram.

According to the charge comparison method formula :

$$PSD = \frac{Q_L}{Q_L + Q_S} \tag{2.1}$$

Q_L and Q_S are charge integrations over long- and short-time windows, respectively, and the PSD is the ratio used to discriminate between neutron and gamma signals. Setting $Q_L = 80$ ns and $Q_S = 28$ ns, gives the CCM scatter plot [13] of the collected signals. As shown in Fig. 4b, the CCM scatter plot has a clear bimodal characteristic, with the upper peak corresponding to the neutron signal distribution and the lower peak corresponding to the gamma signal distribution.

By combining the time-of-flight and charge comparison methods, a neutron/gamma signal dataset consisting of 110,243 gamma signals and 96,562 neutron signals was obtained.

2.2. Part II: Construction of the pile-up pulse dataset

In general, pile-up pulse can be categorized into four types: neutron-neutron pile-up, neutron-gamma pile-up, gamma-neutron pile-up, and gamma-gamma pile-up [8]. To train the network to recognize the four types of piled-up pulses, separate datasets must be created for each signal type. In this study, piled-up pulse signals were simulated by combining the measured neutron and gamma pulse signals. Two signals were randomly selected from the neutron/gamma dataset, randomly offset, and added together to obtain a piled-up pulse signal, as shown in Fig. 5. Repeating this operation results in a dataset with piled-up pulse signals.

To evaluate the performance of the network in recognizing piled-up pulse signals, it is crucial to consider different degrees of pile-up and noise levels [14]. These factors have a significant effect on waveform characteristics and recognition accuracy. Comprehensive datasets were created by simulating different levels of pile-up and noise. The following sections detail the classification of pile-up degrees and noise levels and their impact on signal waveforms.

2.2.1. Pile-up pulses with different degrees of pile-up

The degree of pile-up is defined by the time interval Δt [15,16] between two pulse signals. When Δt is less than 10 ns, the signals overlap almost completely overlap and the information about the trailing edge is lost. When Δt was greater than 25 ns, the signals were almost completely separated, so that the trailing edge information was fully preserved. In this study, the focus was on Δt between 10 and 25ns and defined [10,15) ns as severe pile-up, [15,25) ns as moderate pile-up, and [25,∞) ns as mild pile-up. Fig. 6 shows the waveforms of the piled-up pulses under these classifications using a Pile-up-GG signal selected from the dataset.

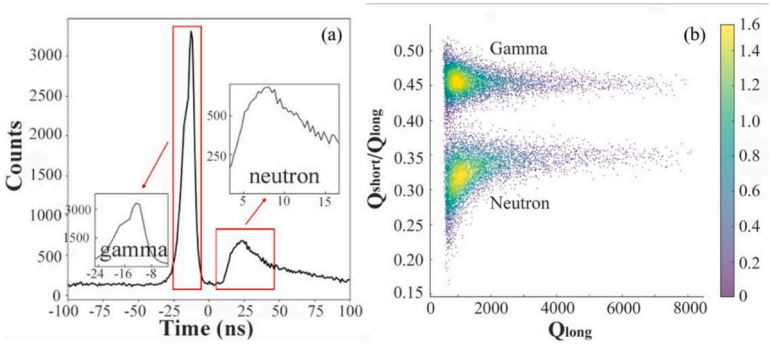

Fig. 4. Time-of-flight spectra (a) and CCM scatter plot (b).

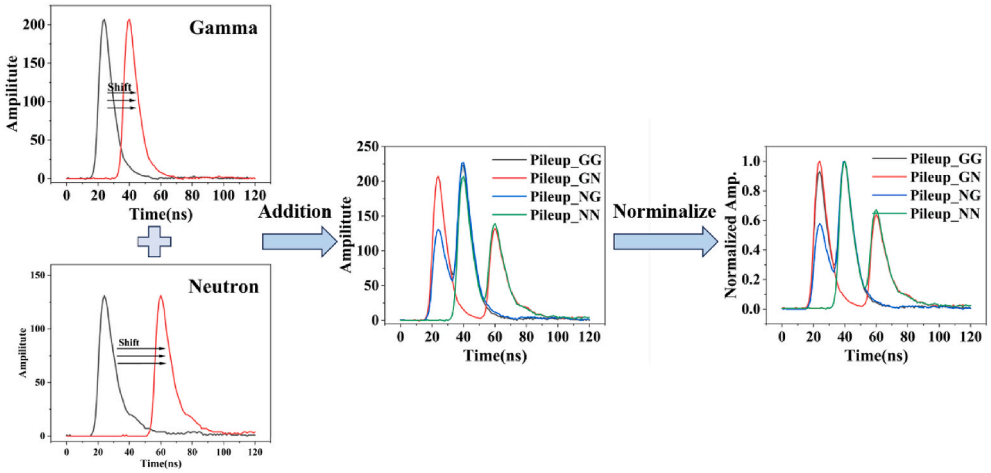

Fig. 5. Generation of a piled-up pulse signal.

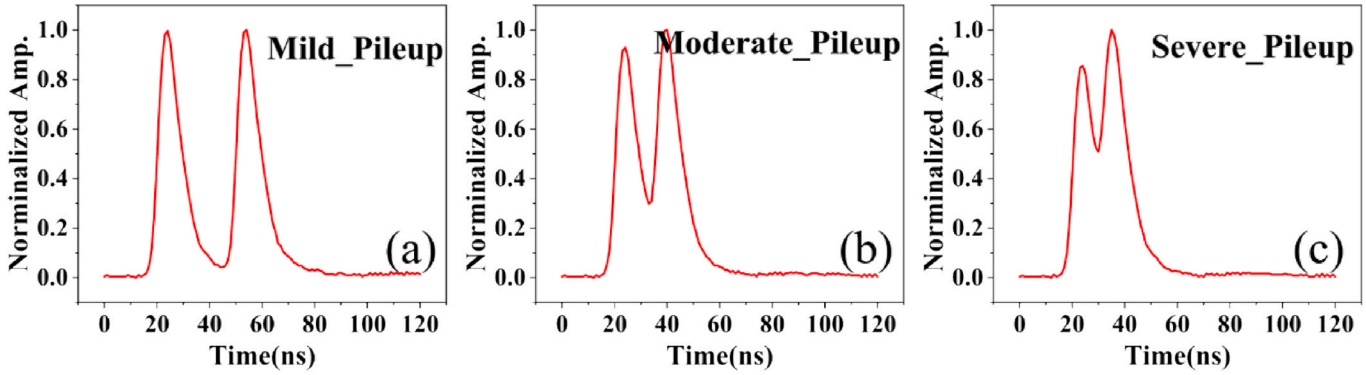

Fig. 6. Piled-up pulse signals with three different degrees of pile-up (a) : Mild_Pileup (b) : Moderate_Pileup (c) : Severe_Pileup

2.2.2. Pile-up pulses with different levels of noise

In radiation detection using liquid scintillator detectors, noise accompanies the signal. The most important types of noise include Poisson noise $\sigma_{Poisson}$, Gaussian noise $\sigma_{Gaussian}$, and Johnson noise $\sigma_{Johnson}$ [17]. The proportion was influenced by the operating temperature and circuit design. The noise standard deviation σ can be expressed as follows:

$$\sigma = \sqrt{{\sigma_{Poisson}}^2 + {\sigma_{Gaussian}}^2 + {\sigma_{Johnson}}^2} \tag{2.2}$$

When the standard deviation of the noise was in the interval (0,0.05), the signal shape remained largely unchanged, with some baseline noise. When the standard deviation of the noise is within the interval [0.05,0.1), the signal shape remains intact but baseline noise increases [18]. When the standard deviation of the noise was in the interval [0.1, 0.15), the signal peak deformed, the trailing edge information was lost, and the baseline noise was very high. When the standard deviation of the noise is in the interval [0.15,∞), most of the waveform information is lost and is not useful for study. This study focused on the standard deviation of the noise in the interval [0.05,0.15), where [0.1,0.15) was defined as severe noise, [0.05,0.1) as moderate noise, and (0,0.05) as mild noise. Fig. 7 shows the waveforms of the piled-up pulses under these classifications using a Pile-up-GG signal selected from the dataset.

The final structure of the dataset and the labels are listed in Table 2.

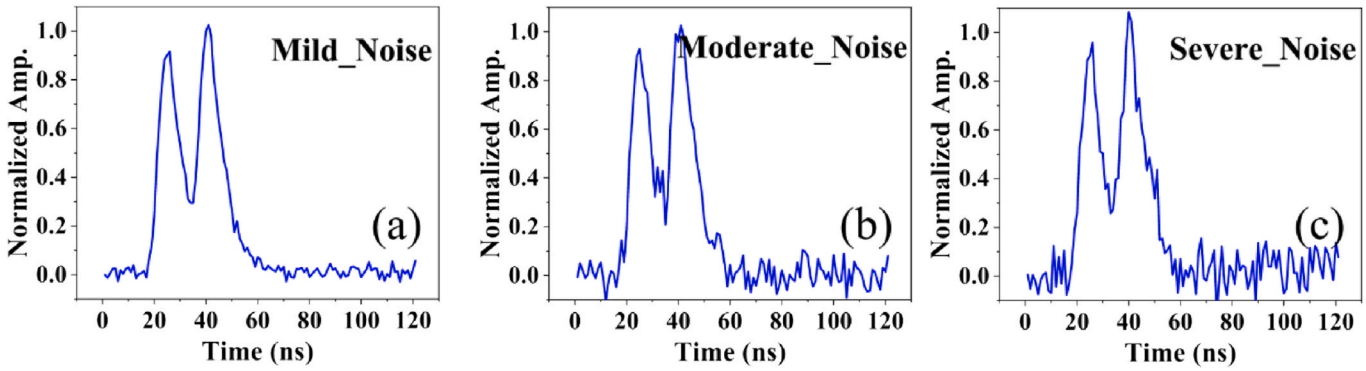

Fig. 7. Piled-up pulse signals with three different noise level (a) : Mild_Noise (b) : Moderate_Noise (c) : Severe_Noise

Table 2
Dataset.

Category	Pile-up Degree	Noise Level	Label	Events
N			111	12,000
G			000	8000
N-G	Mild/Moderate/Severe	Mild/Moderate/Severe	100	9000
N-N			110	9000
G-N			011	9000
G-G			001	9000

2.3. Part III: construction, training, and testing of the neural networks

2.3.1. DenseNet construction

In this study, DenseNet (Fig. 8) for pulse piled-up recognition was constructed. The network consisted of six DenseBlocks and transitionlayers, with each DenseBlock containing four DenseLayers. The ReLu activation function was used throughout, and the loss function was the cross-entropy. All internal network parameters were optimized using Optuna [19].

2.3.2. MMDenseNet construction

MMDenseNet optimizes the recognition of piled-up pulses by selecting different modules based on the pile-up degree P and noise level N of the input pulses. The network consists of nine modules, each tailored to a specific pile-up condition.

When the network receives an input signal, it first applies a peak-detection algorithm to classify it as a neutron or gamma signal. The peak time interval Δt is calculated to estimate P, and the standard deviation σ is computed to estimate N. Based on these estimates, the most suitable network structure is selected.

The signal then enters the selection layer (Fig. 9), which dynamically chooses the optimal combination of DenseBlock and transitionlayer based on the estimated pile-up degree P and noise level N. The selection layer uses a selection function $S(P,N)$ to map the degree of pile-up and noise level to a specific network structure number.

The selected network path processes the signal sequentially through the initial convolutional part, the DenseBlocks, the transitionlayers, and finally arrives at the fully connected layer. Classification was performed using the SoftMax activation function, which outputs a probability distribution over different categories to determine the final classification of the signal.

2.3.3. MMDenseNet-R construction

Building on MMDenseNet, MMDenseNet-R shares the initial convolution and pooling layers to optimize computational efficiency and resource usage, while still maintaining the capability to handle different input features.

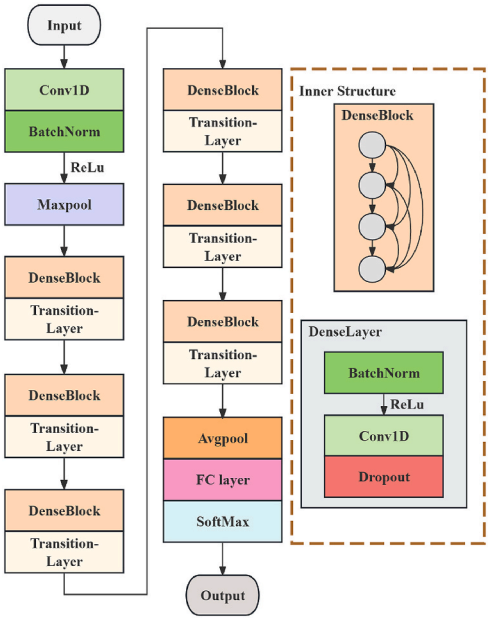

Fig. 8. DenseNet for the recoginition of piled-up pulses.

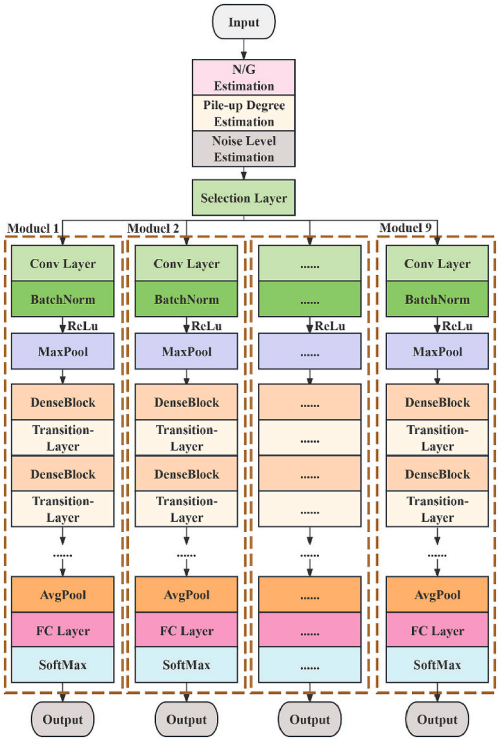

Fig. 9. MMDenseNet for the recoginition of piled-up pulses.

First, the input signal was fed into the network and was assigned a unique identifier (ID). This identifier was used to track the correspondence of the signal in the different paths during parallel processing, thus ensuring the correct assignment of the signal in the subsequent selection layers (Fig. 10).

Next, the signal enters the parallel processing stage, which is divided into two paths: Path 1 for the initial convolutional processing and Path 2 for estimating the degree of pile-up and noise level. In Path 1, the signal successively passes through the Conv1D, BatchNorm, and ReLU activation functions, and then enters the initial pooling layer to reduce the size

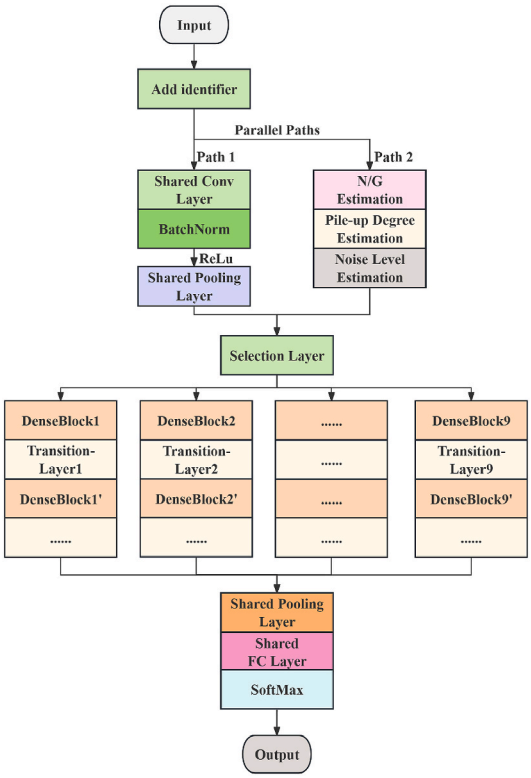

Fig. 10. MMDenseNet-R for the recoginition of piled-up pulses.

Table 3
Structural parameters of MMDenseNet and MMDenseNet-R.

Cases	DenseBlock (a/b)	DenseLayer (a/b)	Growth Rate (a/b)	
1	2/2	3/3	27/31	*a represents
2	3/2	3/3	32/34	MMDenseNet;
3	3/3	4/4	33/31	*b represents
4	3/3	4/4	35/36	MMDenseNet-R
5	3/3	4/4	34/42	
6	4/3	5/5	41/47	
7	4/3	5/5	43/49	
8	4/4	5/5	44/54	
9	4/4	6/6	45/58	

of feature map. These layers can be reused. In Path 2, the signal is subjected to peak-detection to determine whether it is a neutron/gamma signal. Then the peak time interval Δt of the piled-up pulse is calculated to estimate the degree of pile-up P, followed by the calculation of the standard deviation σ to estimate the noise level N.

After parallel processing, the signal enters the selection layer, which uses a selection function $S(P,N)$ to dynamically select the appropriate

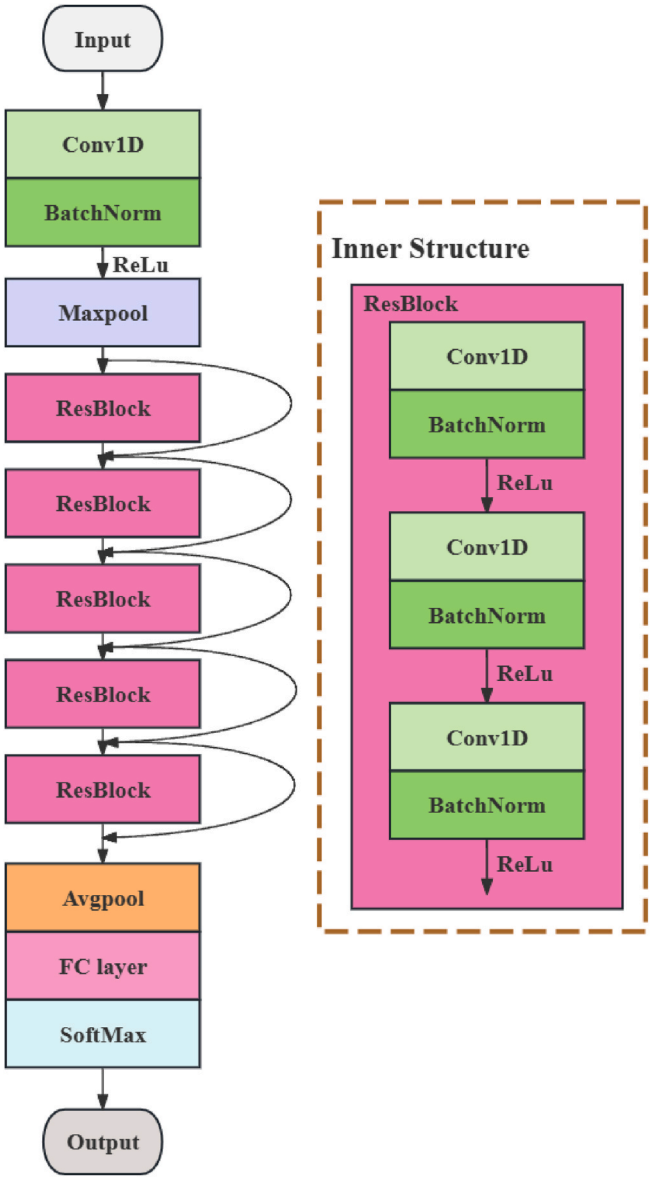

Fig. 11. ResNet for the recognition of piled-up pulses (comparison model).

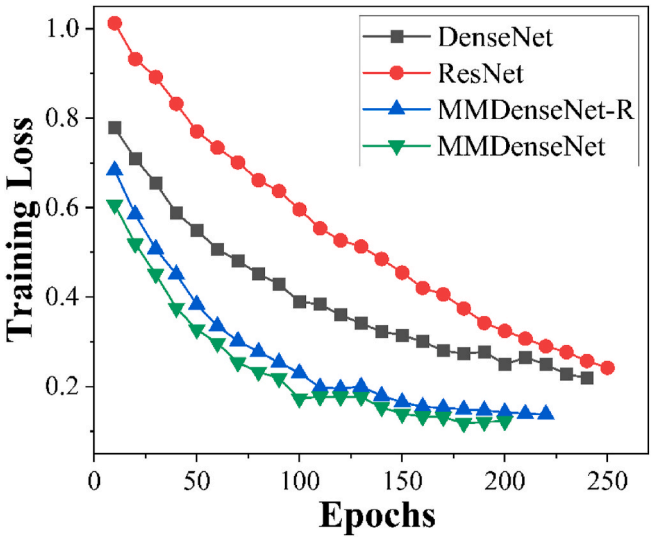

Fig. 12. Average loss curves for ResNet, DenseNet, MMDenseNet, and MMDenseNet-R.

combination of DenseBlock and Transition Layer based on the estimated degree of pile-up P and noise level N. After processing by the DenseBlock and Transition Layer, the signal enters the shared pooling layer and shared fully connected layer. Finally, the signal is classified using the SoftMax activation function, which outputs the probability distribution for different categories to determine the final category of the signal. Some structural parameters are listed in Table 3.

2.3.4. Comparison model & training and testing phase

To intuitively evaluate the pile-up pulse recognition performance of the three DenseNet models constructed in this study, a ResNet model [8] was also built for comparative analysis. The ResNet model consists of five residual blocks, with ReLu as the activation function, and the prediction results are output through AvgPooling at the end. All parameters were optimized using Optuna. The specific structure is shown in Fig. 11.

Different neural networks were trained and tested. The dataset was divided into training, testing, and validation sets in a ratio of 7:1.5:1.5. The average loss curves [21] for the nine pile-up cases are shown in Fig. 12. MMDenseNet and MMDenseNet-R exhibit excellent convergence performance, showing a rapid loss reduction trend from the early stages of training and ultimately achieving a low loss level, with convergence performance significantly better than DenseNet and ResNet.

To make the analysis results more precise, 15 different time-interval collections of piled-up pulses at three noise levels were selected as a test set. Each time interval signal collection consisted of 400 samples. Therefore, the number of test samples for each degree of pile-up was 2000.

To assess the resource utilization and training time of the four network architectures, their FLOPs and parameters were calculated [9, 20] to visualize their resource occupancy. The results showed that MMDenseNet has 4,672,038 parameters and 2,435,325,536 FLOPs, while MMDenseNet-R has 4,530,662 parameters, 97 % of the MMDenseNet total, and 2,314,562,613 FLOPs, 95 % of the MMDenseNet total. By reusing the base layers in MMDenseNet-R, its resource utilization and training time are similar to MMDenseNet, with a slight reduction. Additionally, DenseNet and ResNet have lower resource utilization, with 568,994 and 498,872 parameters, respectively, and FLOPs of 674,234, 801 and 599,682,462. ResNet's parameters and FLOPs account for 88 % and 89 % of DenseNet's total, respectively. Since DenseNet and ResNet do not have the hierarchical structure of MMDenseNet, their training time is shorter, but their accuracy and F1 scores are lower than those of MMDenseNet.

3. Results and discussion

3.1. Evaluation metrics: Accuracy&F1-Score

The evaluation metrics used in this study included accuracy and F1 score [22]. Accuracy and F1 score are commonly used metrics for evaluating model classification performance in machine learning.

The quality of the MMDenseNet pile-up pulse classification performance plays a decisive role in the model's PSD capability. High accuracy indicates that the model can effectively distinguish different types of pulses, while a high F1 score means that the model can not only effectively identify pile-up signals but also has fewer misclassifications of non-target signals.

Accuracy represents the proportion of correctly predicted samples to the total number of samples and is calculated as follows:

$$\mathrm{Acc} = \frac{\mathrm{TP} + \mathrm{TN}}{\mathrm{TP} + \mathrm{FN} + \mathrm{FP} + \mathrm{TN}} \tag{3.1}$$

In pulse pile-up recognition, accuracy reflects the overall performance of the model in distinguishing different pulse categories (such as neutron, gamma, and their combinations). However, accuracy does not comprehensively measure the model's performance, especially in cases of class imbalance. For example, if the model accurately predicts non-pile-up pulses but performs poorly in detecting overlapping pulses (such as neutron-neutron or neutron-gamma), the accuracy may appear high, but this does not reflect the model's effectiveness in complex signal processing.

Recall represents the proportion of true positive samples to actual positive samples and is calculated as follows:

$$\mathrm{Recall} = \frac{\mathrm{TP}}{\mathrm{TP} + \mathrm{FN}} \tag{3.2}$$

In pulse pile-up recognition, recall helps assess the model's sensitivity in identifying pile-up signals (such as NN or NG). A high recall indicates that the model can effectively detect more samples that actually belong to pile-up pulses, which is crucial for ensuring that no important signals are missed.

Precision represents the proportion of true positive samples in the predicted positive samples, and is calculated as follows:

$$\mathrm{Precision} = \frac{\mathrm{TP}}{\mathrm{TP} + \mathrm{FP}} \tag{3.3}$$

In the task of pulse pile-up recognition, precision reflects the model's accuracy in determining whether a pulse belongs to a specific category. If the model frequently misclassifies non-pile-up pulses as pile-up pulses, the precision will decrease, indicating that the model's capability in handling complex signals is insufficient.

The F1-score is the harmonic mean of precision and recall and represents the balance between the two. The F1 score was calculated as follows:

$$\mathrm{F1} = 2^{*}\frac{\mathrm{Precision}^{*}\mathrm{Recall}}{\mathrm{Precision} + \mathrm{Recall}} \tag{3.4}$$

In pulse pile-up recognition, the F1 score provides a more insightful perspective for evaluating the model's overall performance in identifying and classifying overlapping signals. Especially when handling complex signals like NN and NG, the F1 score better reflects the model's performance in avoiding missed detections and misclassifications. For instance, if the model can identify most NN signals but misses some actual NN samples (leading to low recall), or incorrectly predicts some NG signals as NN (leading to low precision), the F1 score will be significantly affected, providing direction for further optimization of the model.

In this study, True Positive (TP) represents samples that are correctly classified as a specific category (N, G, NN, NG, GN, GG). In cases where the actual category is NN and the model also predicts NN, the sample is counted as a TP. False Negative (FN) denotes samples that belong to a particular category but are incorrectly classified as another. In instances where the actual category is NN but the model predicts NG, this sample is considered an FN. False Positive (FP) represents samples from other categories that are incorrectly classified as the target category, when the actual category is NG but the model predicts NN, this sample is counted as an FP. True Negative (TN) represents samples that do not belong to the target category and are correctly identified as not belonging to it; if the actual category is NG and the model predicts a category other than NN, this sample is counted as a TN.

3.2. Evaluation on model performance in nine pile-up conditions

In this study, a subset of samples from 15 different time intervals were selected from the test set, with 400 piled-up pulse samples for each noise level in each time interval. This allowed for a performance comparison between DenseNet, MMDenseNet, and MMDenseNet-R under different pile-up conditions, as shown in Fig. 13. The results indicate that both MMDenseNet and MMDenseNet-R generally perform better than DenseNet, especially as the time intervals increase. When the time

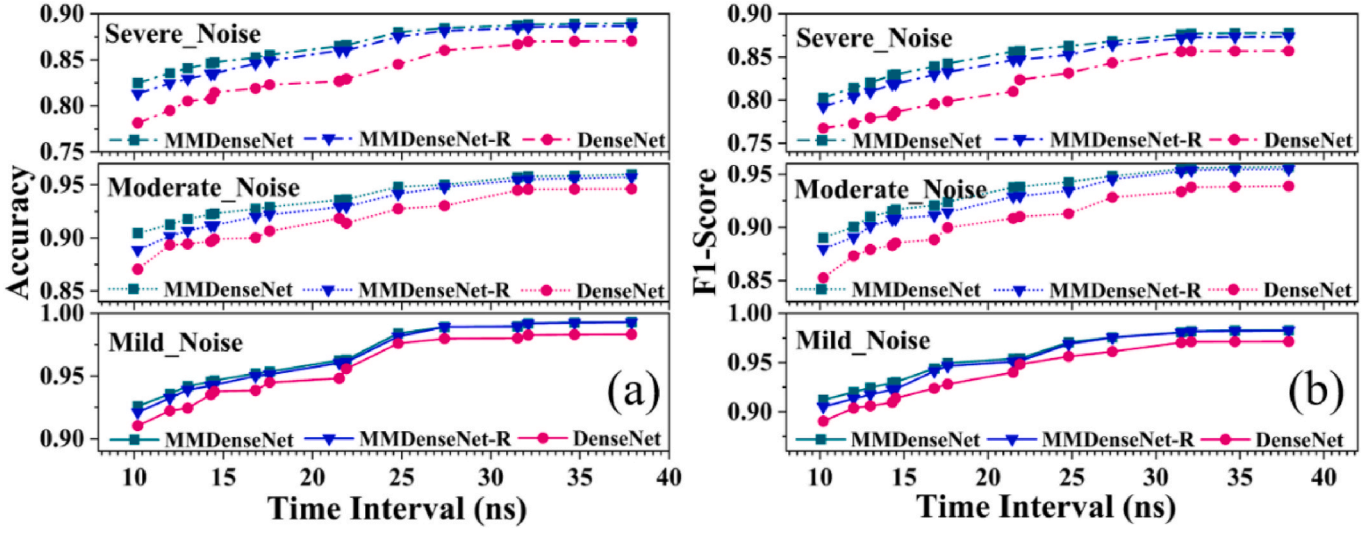

Fig. 13. Accuracy(a) and F1-Score(b) of DenseNet and MMDenseNet/MMDenseNet-R under different Noise Levels (the solid line represents mild noise, the dashed line represents moderate noise, and the dashed-dotted line represents severe noise.).

interval exceeded 25 ns, under mild noise conditions, MMDenseNet and MMDenseNet-R achieved near-perfect accuracy at the lightest pile-up level, reaching 0.993 and 0.9928, respectively. The accuracy of DenseNet also improved with longer intervals but remained lower overall, with a maximum of 0.9855. Noise has a stronger influence on the accuracy of DenseNet, whereas the MMDenseNet models show greater robustness and resistance to noise. Even in high noise and under the most severe pile-up conditions, MMDenseNet and MMDenseNet-R maintained higher accuracy (0.825 and 0.8131, respectively) than DenseNet (0.7815), indicating better recognition reliability.

3.3. Comparing performance with ResNet

The piled-up pulse recognition performance of three DenseNet models was compared with the ResNet structure. Each noise level had 5000 signal samples as test samples to evaluate the accuracy and F1 score of the network models. MMDenseNet performed consistently better than the other models at all noise levels, with ResNet performing the worst. MMDenseNet showed a 3–8% improvement in accuracy and F1 score over ResNet, as shown in Fig. 14.

Under mild noise, MMDenseNet achieved an accuracy of 0.9867 and an F1-Score of 0.9785, outperforming ResNet by 3.2 % and 2.8 %, respectively. In the presence of severe noise, the accuracy of MMDenseNet was 0.8752 and F1-Score of 0.8641, outperforming those of ResNet by 7.8 % and 7.0 %, respectively. DenseNet models with their modular design, showed better resistance to noise, with accuracy decreasing by only 10 % in mild to severe noise, while maintaining an accuracy above 0.85. In contrast, the non-modular DenseNet and ResNet models saw accuracy drop by almost 15 % to below 0.85.

Despite demonstrating good recognition performance under low noise and low pile-up conditions, ResNet's recognition ability consistently lags behind DenseNet and MMDenseNet/MMDenseNet-R. As noise levels increase and pile-up severity rises, ResNet's performance declines significantly faster than the other three models, resulting in a marked reduction in recognition accuracy.

4. Conclusions

In this study, the problem of piled-up pulses in the neutron-gamma discrimination domain was investigated and a multi-module hierarchical neural network model was proposed to significantly improve the classification performance of a single neural network in handling complex signal recognition scenarios.

The proposed MMDenseNet and MMDenseNet-R models showed comparable resource utilization, with MMDenseNet showing slightly superior recognition performance. MMDenseNet achieved excellent performance under all nine pile-up conditions in this study, whereas ResNet performed significantly worse than DenseNet and MMDenseNet/MMDenseNet-R under severe pile-up and noise conditions. Under the most challenging conditions, the accuracy of ResNet was only 0.8122, which was slightly lower than DenseNet's accuracy of 0.8388 and significantly lower than MMDenseNet and MMDenseNet-R's accuracy of 0.8752 and 0.8677, respectively. DenseNet exhibited better stability for neutron/gamma piled-up pulse recognition under complex conditions, whereas MMDenseNet showed higher resistance to noise and interference than DenseNet, with its modular design.

Based on the comparison of accuracy and F1 score, MMDenseNet/MMDenseNet-R demonstrates superior recognition and classification performance, accurately distinguishing pile-up pulse signals from neutron and gamma signals, reflecting its excellent PSD capabilities.

Due to the lack of modular design, ResNet and DenseNet have simpler structures, with parameter counts at only about 25 % of those in the MMDenseNet structure. This leads to lower resource utilization and shorter training times, but they show certain limitations under complex pile-up conditions and high noise levels. Both training loss and performance metrics, including accuracy and F1 score, are significantly lower than those of MMDenseNet.

In the environment of the Am-Be source from the State Key Laboratory of Nuclear Physics and Technology at Peking University, due to the high-count rate of the detection environment, the pile-up pulse signals detected by the EJ301 detector significantly increased. Under these conditions, the frequency of the detector discarding pile-up pulses continues to rise, leading to cumulative dynamic deadtime in the system, which severely affects detection efficiency. The MMDenseNet model proposed in this paper successfully identifies pile-up pulses and restores data from some of the pile-up pulse signals that would otherwise have been discarded, thereby increasing the number of useful pulses. By using this model, the system's processing time for pile-up pulses is reduced, which in turn decreases detector and electronic dynamic deadtime.

Under similar conditions to mainstream pile-up pulse discrimination methods [8,17,23], the MMDenseNet/MMDenseNet-R models proposed

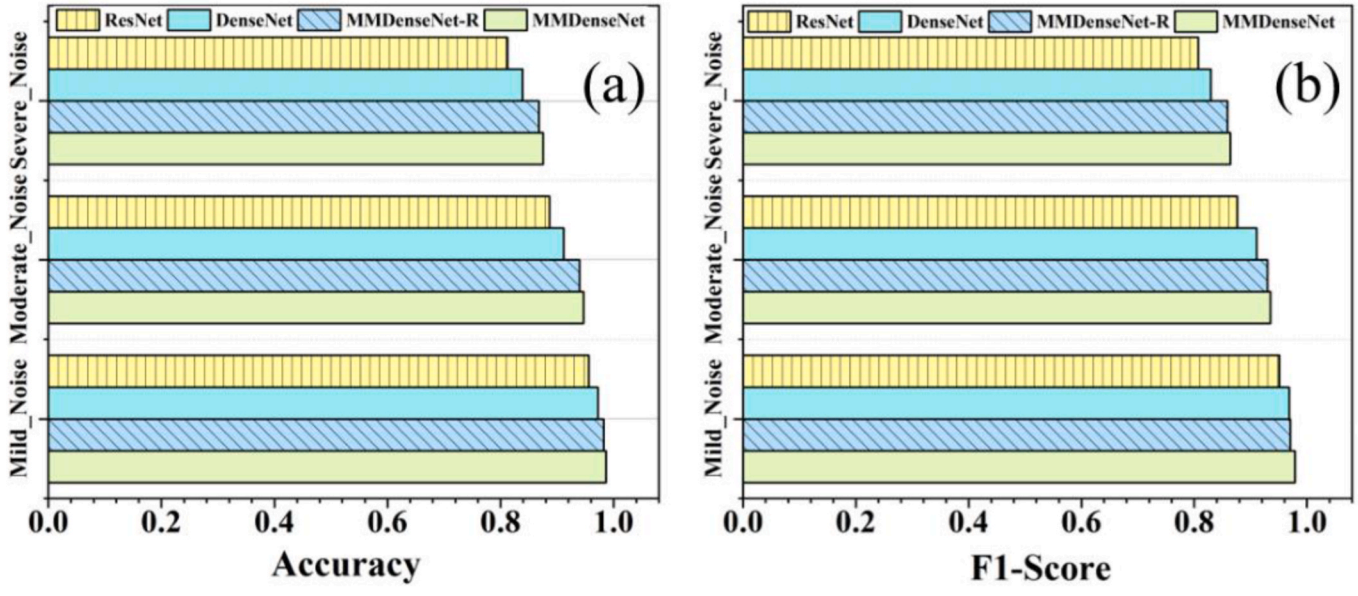

Fig. 14. Accuracy(a) and F1-Score(b) of ResNet, DenseNet and MMDenseNet/MMDenseNet-R under three Noise Levels.

in this paper are currently applicable to two-pulse pile-up scenarios and demonstrate good performance in pile-up pulse recognition and PSD. In practical detection environments, cases of multiple pulse pile-up may also occur. When multiple pulses enter the detector within the same time window, they form a multi-pulse pile-up. Although the occurrence of multi-pulse pile-up is significantly lower than that of two-pulse pile-up, it remains a new research topic worthy of further investigation.

CRediT authorship contribution statement

Ye Pan: Writing – original draft, Conceptualization. **Pin Gong:** Writing – review & editing. **Zhimeng Hu:** Writing – review & editing, Conceptualization. **Zeyu Wang:** Writing – review & editing. **Dajian Liang:** Writing – review & editing. **Cheng Zhou:** Funding acquisition. **Xiaoxiang Zhu:** Funding acquisition. **Xiaobin Tang:** Writing – review & editing.

Declaration of competing interest

The authors declare that they have no known competing financial interests or personal relationships that could have appeared to influence the work reported in this paper.

Acknowledgements

This work was supported by the National Natural Science Foundation of China (Grant No. 12375297, 12105144), and the Primary Research and Development Plan of Jiangsu Province (Grant No. BE2023816, BE2022846).

References

[1] L. Chang, Y.D. Liu, L. Du, et al., Pulse shape discrimination and energy calibration of EJ-301 liquid scintillation detector, Nucl. Tech. 38 (2015) 020501, https://doi.org/10.11889/j.0253-3219.2015.hjs.38.020501 (in Chinese).

[2] S.-X. Liu, et al., Performance of real-time neutron/gamma discrimination methods, Nucl. Sci. Tech. 34 (1) (Jan. 2023) 8, https://doi.org/10.1007/s41365-022-01160-5.

[3] A. Yamazaki, et al., Neutron–gamma discrimination based on pulse shape discrimination in a Ce:LiCaAlF6 scintillator, Nucl. Instrum. Methods Phys. Res. Sect. Accel. Spectrometers Detect. Assoc. Equip. 652 (1) (Oct. 2011) 435–438, https://doi.org/10.1016/j.nima.2011.02.064.

[4] M. Nakhostin, P.M. Walker, Application of digital zero-crossing technique for neutron-gamma discrimination in liquid organic scintillation detectors, Nucl. Instrum. Methods Phys. Res. Sect. -Accel. Spectrometers Detect. Assoc. Equip. 621 (1–3) (Sep. 2010) 498–501, https://doi.org/10.1016/j.nima.2010.06.252.

[5] Z. Zihao, J. Geng, W. Jiang, A time series classification method based on 1DCNN-FNN, in: 2021 33rd Chinese Control and Decision Conference (CCDC), IEEE, Kunming, China, May 2021, pp. 1566–1571, https://doi.org/10.1109/CCDC52312.2021.9602164.

[6] K. He, X. Zhang, S. Ren, J. Sun, Deep residual learning for image recognition, in: *2016 IEEE Conference On Computer Vision and Pattern Recognition (CVPR)*, Las Vegas, NV, USA, IEEE, Jun. 2016, pp. 770–778, https://doi.org/10.1109/CVPR.2016.90.

[7] G.P. Westphal, High rate gamma-spectroscopy and related problems, J. Radioanal. Chem. 61 (1–2) (Mar. 1981) 111–119, https://doi.org/10.1007/BF02517402.

[8] H. Song, C. Yang, B. Yu, X. Li, T. Hu, L. Sun, Neutron-gamma events discrimination under complex circumstances using ResNet, J. Instrum. 18 (1) (Jan. 2023) P01007, https://doi.org/10.1088/1748-0221/18/01/P01007.

[9] G. Huang, Z. Liu, L. van der Maaten, K.Q. Weinberger, Densely connected convolutional networks, arXiv: arXiv:1608.06993 (2018). http://arxiv.org/abs/1608.06993. (Accessed 17 June 2024).

[10] U. Boesl, Time-of-Flight Mass spectrometry: introduction to the basics, Mass Spectrom. Rev. 36 (1) (Feb. 2017) 86–109, https://doi.org/10.1002/mas.21520.

[11] H. Bai, et al., Calibration of an EJ309 liquid scintillator using an AmBe neutron source, Nucl. Instrum. Methods Phys. Res. Sect. Accel. Spectrometers Detect. Assoc. Equip. 863 (Aug. 2017) 47–54, https://doi.org/10.1016/j.nima.2017.04.028.

[12] H. Bai, et al., A method to calibrate the n-γ discrimination property of scintillators in low energy region, Appl. Radiat. Isot. 167 (Jan. 2021) 109447, https://doi.org/10.1016/j.apradiso.2020.109447.

[13] J.M. Adams, G. White, A versatile pulse shape discriminator for charged particle separation and its application to fast neutron time-of-flight spectroscopy, Nucl. Instrum. Methods 156 (3) (Nov. 1978) 459–476, https://doi.org/10.1016/0029-554X(78)90746-2.

[14] S. Dési, New noise reduction techniques processing nuclear detector signals, Nucl. Instrum. Methods Phys. Res. Sect. -Accel. Spectrometers Detect. Assoc. Equip. 521 (2–3) (Apr. 2004) 611–613, https://doi.org/10.1016/j.nima.2003.11.190.

[15] S. Cheng, B. Pierson, S. Pommé, M. Flaska, Time interval distributions of nuclear events in a digital spectrometer, Nucl. Instrum. Methods Phys. Res. Sect. Accel. Spectrometers Detect. Assoc. Equip. 1063 (Jun. 2024) 169218, https://doi.org/10.1016/j.nima.2024.169218.

[16] S. Pommé, B. Denecke, J.P. Alzetta, Influence of pileup rejection on nuclear counting, viewed from the time-domain perspective, Nucl. Instrum. Methods Phys. Res. Sect. -Accel. Spectrometers Detect. Assoc. Equip. 426 (2–3) (May 1999) 564–582, https://doi.org/10.1016/S0168-9002(99)00016-9.

[17] Y. Ma, et al., A method for discriminating neutron and gamma waveforms based on a comparison of differences between pulse feature heights, J. Radioanal. Nucl. Chem. 333 (1) (Jan. 2024) 375–386, https://doi.org/10.1007/s10967-023-09280-x.

[18] M. Kafaee, A. Moussavi-Zarandi, Baseline restoration and pile-up correction based on bipolar cusp-like shaping for high-resolution radiation spectroscopy, J. Kor. Phys. Soc. 68 (8) (Apr. 2016) 960–964, https://doi.org/10.3938/jkps.68.960.

[19] T. Akiba, S. Sano, T. Yanase, T. Ohta, M. Koyama, Optuna: a next-generation hyperparameter optimization framework, in: KDD'19: PROCEEDINGS OF THE 25TH ACM SIGKDD INTERNATIONAL CONFERENCCE ON KNOWLEDGE DISCOVERY AND DATA MINING, Assoc Computing Machinery, New York, 2019, pp. 2623–2631, https://doi.org/10.1145/3292500.3330701.

[20] N. Ma, X. Zhang, H.-T. Zheng, J. Sun, ShuffleNet V2: practical guidelines for efficient CNN architecture design, in: P.T. XIV, V. Ferrari, M. Hebert, C. Sminchisescu, Y. Weiss (Eds.), COMPUTER VISION - ECCV 2018, Lecture Notes in Computer Science, vol. 11218, Springer International Publishing Ag, Cham, 2018, pp. 122–138, https://doi.org/10.1007/978-3-030-01264-9_8.

[21] J.-Y. Zhu, T. Park, P. Isola, A.A. Efros, Unpaired image-to-image translation using cycle-consistent adversarial networks, in: 2017 IEEE INTERNATIONAL CONFERENCE ON COMPUTER VISION (ICCV), IEEE, New York, 2017, pp. 2242–2251, https://doi.org/10.1109/ICCV.2017.244. IEEE International Conference on Computer Vision.

[22] D. Li, W. Li, Y. Zhao, X. Liu, The analysis of deep learning recurrent neural network in English grading under the internet of things, IEEE Access 12 (2024) 44640–44647, https://doi.org/10.1109/ACCESS.2024.3380480.

[23] J. Han, et al., Pulse characteristics of CLYC and piled-up neutron–gamma discrimination using a convolutional neural network, Nucl. Instrum. Methods Phys. Res. Sect. A Accel. Spectrom. Detect. Assoc. Equip. 1028 (2022) 166328.